JTTEE5 9:513-519

Improving Corrosion Properties of High-Velocity Oxy-Fuel Sprayed Inconel 625 by Using a High-Power Continuous Wave Neodymium-Doped Yttrium Aluminum Garnet Laser

J. Tuominen, P. Vuoristo, T. Mäntylä, M. Kylmälahti, J. Vihinen, and P.H. Andersson

(Submitted 21 January 2000)

Thermal spray processes are widely used to protect materials and components against wear, corrosion and oxidation. Despite the use of the latest developments of thermal spraying, such as high-velocity oxy-fuel (HVOF) and plasma spraying, these coatings may in certain service conditions show inadequate performance, *e.g.*, due to insufficient bond strength and/or mechanical properties and corrosion resistance inferior to those of corresponding bulk materials. The main cause for a low bond strength in thermal-sprayed coatings is the low process temperature, which results only in mechanical bonding. Mechanical and corrosion properties typically inferior to wrought materials are caused by the chemical and structural inhomogeneity of the thermal-sprayed coating material. To overcome the drawbacks of sprayed structures and to markedly improve the coating properties, laser remelting of sprayed coatings was studied in the present work. The coating material was nickel-based superalloy Inconel 625, which contains chromium and molybdenum as the main alloying agents. The coating was prepared by HVOF spraying onto mild steel substrates. High-power continuous wave Nd:YAG laser equipped with large beam optics was used to remelt the HVOF sprayed coating using different levels of power and scanning speed. The coatings as-sprayed and after laser remelting were characterized by optical microscopy and scanning electron microscopy (SEM). Laser remelting resulted in homogenization of the sprayed structure. This strongly improved the performance of the laser-remelted coatings in adhesion, wet corrosion, and high-temperature oxidation testing. The properties of the laser-remelted coatings were compared directly with the properties of as-sprayed HVOF coatings and with plasma-transferred arc (PTA) overlay coatings and wrought Inconel 625 alloy.

Keywords corrosion, HVOF, Inconel 625, laser remelting, Nd:YAG laser

1. Introduction

High-strength, oxidation-, and corrosion-resistant nickel-based superalloy Inconel 625 (INCO Alloys International, Huntington, WV) is widely used as a wrought material and thermally sprayed coating in applications where a variety of aggressive corrosive agents (chlorides, sulfides, *etc.*) are present at low or high temperatures. Economically, it makes sense to manufacture components with excellent resistance to corrosion and oxidation by using a relatively expensive superalloy as a thermal spray coating instead of the corresponding bulk material. However, in spite of the efforts made to improve present spraying techniques such as high-velocity oxy-fuel (HVOF), atmospheric plasma spraying, and VPS, thermal spray coatings still exhibit certain drawbacks compared to bulk material. In thermal spraying, the spray material particles are exposed to air atmosphere, which results in oxidation in the coating structure. Due to low process temperature, only mechanical bonding is obtained between the coating and the substrate. In addition, thermal spray coatings may include unmelted particles, weak splat boundaries, residual porosity, and cracks, resulting in an inhomogeneous structure, which may be detrimental to the corrosion performance.

Laser surface post-treatment can offer a controlled way to improve the properties of the sprayed coatings without changing the substrate properties. Laser surface modification of the nickel-based alloys and coatings has been reported since the late 1970s.[1] Several studies have shown that laser surface melting can be used to increase the density of the relatively porous plasma-sprayed nickel-based coatings.[2,3,4] Rapid solidification inherent to laser-treated surfaces results in coatings with columnar and dendritic microstructures.[5] On the other hand, the choice of inappropriate laser processing parameters can lead to certain defects such as cracks, porosity, and excessive dilution from substrate to coating, which all decrease the properties of the coating.[6]

The laser device usually employed for surface treatments has been a CO_2 laser, because of its high power range (up to 25 to 45 kW). This laser, both in pulsed and continuous wave modes, has been used successively in surface homogenization (remelting),[7] cladding,[8] glazing,[3] and alloying[9] of nickel-based alloys with quite narrow beam widths (up to 3 mm). In recent years, the de-

J. Tuominen, P. Vuoristo, T. Mäntylä, and **M. Kylmälahti,** Institute of Materials Science, Tampere University of Technology, FIN 33101 Tampere, Finland; and **J. Vihinen** and **P.H. Andersson,** Institute of Production Engineering, Tampere University of Technology, FIN 33101 Tampere, Finland. Contact e-mail: jjtuomin@butler.cc.tut.fi.

Table 1 Nominal composition of spray powder in wt.%

Powder	Ni	Cr	Mo	Nb	Fe	Si
IN 625	Bal	21.5	9.0	3.6	2.5	0.25

Table 2 HVOF spraying parameters

Oxygen (L/min)	150	Feed rate (g/min)	60
Propane (L/min)	70	Spray distance (mm)	230
Air (L/min)	360	Surface speed (m/min)	100
Carrier gas		Traverse speed (mm/r)	5
Nitrogen (L/min)	13		

velopment in neodymium-doped yttrium aluminum garnet (Nd:YAG) laser technology has resulted in continuous wave multikilowatt (up to 5 kW) high-power devices, which have certain advantages compared to CO_2 lasers. Due to the shorter wavelength of radiation (1.06 μm versus 10.6 μm) the laser beam can be transmitted through optical fiber, which offers great opportunities to utilize industrial robots and treat components remote from the laser source. Moreover, most of the metals absorb shorter wavelength radiation more efficiently, enabling, together with high power, the use of wide beam optics.

In this paper, metallurgical properties of the laser-remelted coating using wide beam width (10 mm) and HVOF-sprayed coating are examined. In addition, corrosion resistance in 3.5 wt.% NaCl and high-temperature oxidation of the remelted and HVOF-sprayed coatings are examined and compared to the wrought Inconel 625 and plasma-transferred arc (PTA) coatings.

2. Experimental

Inconel 625 coatings were produced by using a Diamond Jet Hybrid 2700 HVOF spray process manufactured by Sulzer Metco. The spray powder was commercial Inconel 625 (Ni-Cr-Mo) superalloy (–45 μm), the chemical composition of which is shown in Table 1. The Diamond Jet Hybrid 2700 is considered to be a third generation HVOF process equipped with a converging/diverging nozzle, which enhances the velocity of the powder particles, generating very high coating density and a low amount of oxidation. Furthermore, the homogeneity of the HVOF-sprayed coating quality and the uniform thickness of the coating are features that favor subsequent laser remelting. The spraying parameters used are presented in Table 2. The substrate material was unalloyed low carbon steel Fe 37 with dimensions of 100×60 mm and a thickness of 8 mm. Before spraying, the substrates were roughened by alumina (Al_2O_3) grit blasting to improve the bond strength between substrate and coating. The thickness of the obtained coatings was approximately 300 μm.

The remelting experiments of the sprayed coatings were conducted with a 4 kW continuous wave optical fiber coupled HAAS HL 4006 D Nd:YAG laser. The processing end of the fiber was equipped with hardening optics, which consists of a collimator and an integrating mirror having an effective focal length of 100 mm. The rectangular shape of the delivering beam was defocused to a spot size of 10×8 mm, enabling melt widths of 10 mm. Coating samples were mounted on a moving, numerically controlled x-y table below the fixed laser processing head.

Table 3 Laser parameters used with coating remelting

Power (W)	Traverse speed (mm/min)	Beam width (mm)	Specific energy (J/mm^2)
2250	600	10	22.5
2000	500	10	24.0
2250	500	10	27.0
2500	500	10	30.0
2250	400	10	33.8

To remelt the entire surface area of the HVOF-sprayed coating, a series of overlapping passes were made using different levels of laser power (W) and scanning speed (mm/min), as shown in Table 3. An overlap of 2 mm was used. Nitrogen shield gas was blown through the hardening optics and from the distinct gas nozzle onto the workpiece to minimize the oxidation of the sample and to protect the mirror in the processing head.

The coating microstructures were characterized longitudinally and transversely by optical microscopy and scanning electron microscopy (SEM). To reveal the obtained microstructures, the coatings were etched with a solution consisting of 15 ml HCl, 10 ml CH_3COOH, and 10 ml HNO_3.

In immersion tests, the samples were exposed to 3.5 wt.% NaCl solution at room temperature for 7 days. At the same time, open circuit potential of the coating/substrate system was measured with respect to the Ag/AgCl reference electrode using a high resistance voltmeter. The area exposed to the electrolyte was 7.6 cm^2, which represents 13% of the entire surface of the sample. The exposed area was restricted by a plastic tube, which was glued to the surface of the sample and was filled with the electrolyte.

Cyclic potentiodynamic polarization measurements were performed in 3.5 wt.% NaCl electrolyte at room temperature using a flat specimen cell from EG&G PARC in which a 1 cm^2 area of coating surface was exposed to NaCl solution. The corrosion cell was a glass cylinder horizontally sandwiched between two flat blocks. One block had a circular opening 11 mm in diameter against which the coating surface to be studied was pressed. The point of contact between corrosion cell and coating surface was sealed with a plastic gasket. The potentials were measured with respect to the Ag/AgCl reference electrode, which was connected to the sample through a salt bridge, after 5 min immersion in the electrolyte. A platinum electrode was used as a counter electrode. The scanning speed was 0.5 mV/s.

High-temperature oxidation tests were carried out in a tube furnace at 800 °C in air atmosphere for a period of 100 h. The oxidized coating samples were then mounted in epoxy for microstructural studies and for the thickness measurements of the formed oxide layer.

3. Results and Discussion

The laser parameters shown in Table 3 were high enough to melt fully the HVOF-sprayed coating. The melt depth of the samples was noted to increase from 260 to 840 μm when the specific energy absorbed by the surface was increased by slowing down the traverse speed or raising the power (Fig. 1). When the thickness of the sprayed coating was measured to be approximately 300 μm before laser treatment, it can be said that samples

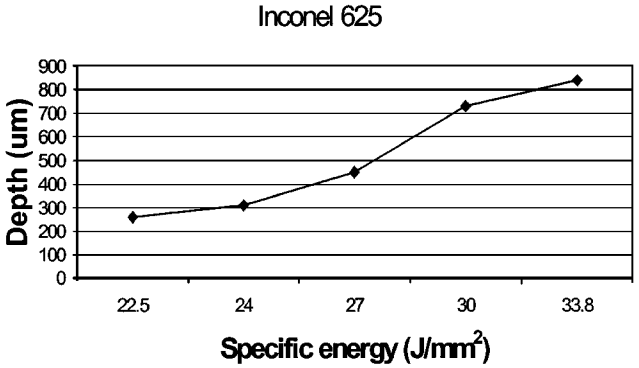

Fig. 1 Melt depth of laser-remelted Inconel 625 coatings as a function of specific energy. Original coating thickness was 300 μm

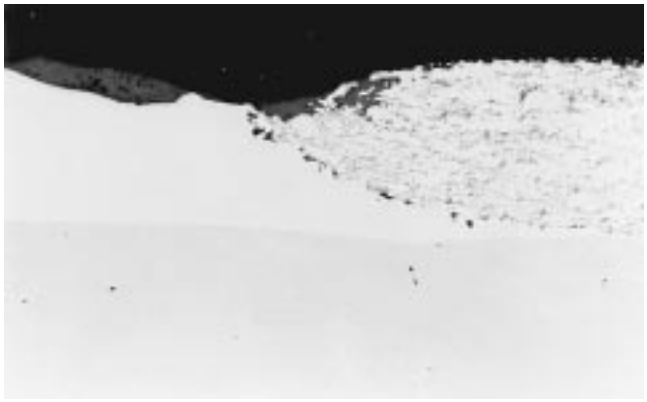

Fig. 2 Optical micrograph of remelted (2250 W, 500 mm/min) and HVOF-sprayed coating (transverse direction), in which the irregular shape of the surface and slag formation can be seen. Coating thickness is 300 μm

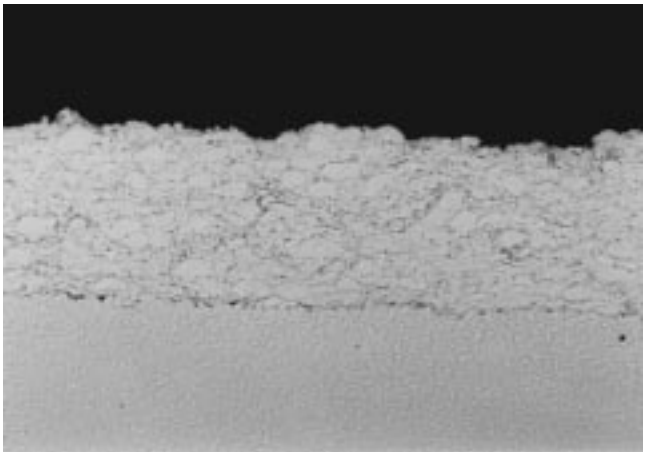

Fig. 3 Optical micrograph of HVOF-sprayed Inconel 625 coating. Oxide layers at splat boundaries can be seen. Coating thickness is 300 μm

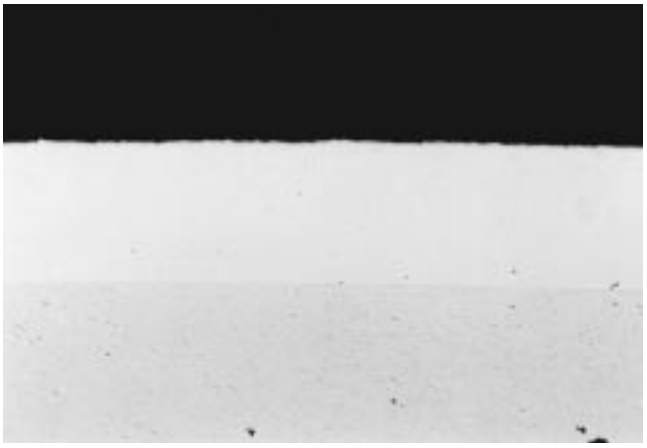

Fig. 4 Optical micrograph of remelted (2250 W, 500 mm/min) Inconel 625 coating (longitudinal direction). Coating thickness is 400 μm after remelting

treated with parameters 2250 W, 600 mm/min and 2000 W, 500 mm/min showed the melt depths close to the original thickness of the coating. Laser parameters with higher specific energy produced melt depths markedly higher than the thickness of 300 μm, indicating high dilution and mixing between coating and substrate. It was also noted that the obtained surface smoothness was strongly influenced by laser power and traverse speed. With low traverse speed and/or high power, the melt pool solidified to the shape in which the material was clustered from both sides of the track to the center of the track, generating an irregular surface (Fig. 2). According to Mahank *et al.*,[3] this happens because of surface tension forces in the melt pool. Samples treated with high specific energy also exhibited strong slag formation, particularly within the 2 mm area where the adjacent beams were overlapped.

The microstructures of the as-sprayed and laser-remelted coatings are shown in Fig. 3 and 4.

The layered microstructure in this HVOF-sprayed coating is clearly seen. Layers of oxides at intersplat boundaries, as seen in Fig. 3, are typical for metallic alloys. During spraying, molten powder particles are exposed to air and are oxidized in flight to the substrate. Oxidation can also occur at the exposed surface of splats prior to deposition of the subsequent layer.[10] The microstructure of the as-sprayed coating also seems to be of relatively low porosity and without cracks.

The coatings obtained using laser remelting are metallurgically dense and free of cracks and porosity, as seen in Fig. 4. It can be seen that the metallurgical bond between coating and substrate was formed, indicating better adherence than in the case of as-sprayed coating.

Figure 5 shows the etched microstructure of a laser-remelted Inconel 625 coating. The microstructure consists of fine cells and columnar grains resulting from the rapid solidification typical for the laser remelting process. The columnar grain growth has originated from the substrate by self-quenching and followed the direction of liquid/solid interface propagation from the substrate/coating interface to the coating surface.

3.1 Immersion Test/OCP

In the case of the HVOF-sprayed coating, the open circuit potential value versus Ag/AgCl reference electrode started to change to a more negative direction immediately after exposure

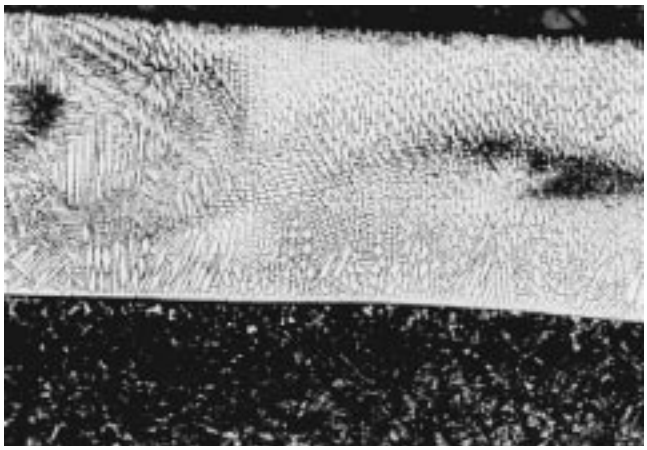

Fig. 5 Optical micrograph of remelted (2250 W, 500 mm/min) and etched Inconel 625 coating (longitudinal direction). Columnar grains and cells can be seen. Coating thickness is 400 μm

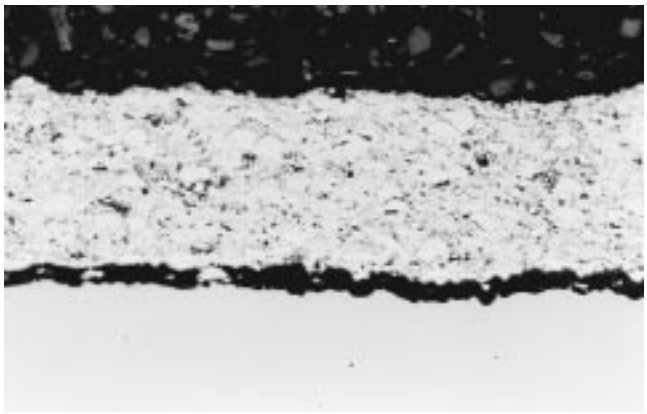

Fig. 6 Optical micrograph of HVOF-sprayed Inconel 625 coating after one week immersion test in 3.5 wt.% NaCl. Electrolyte has corroded the substrate and the coating selectively. Coating thickness is 300 μm

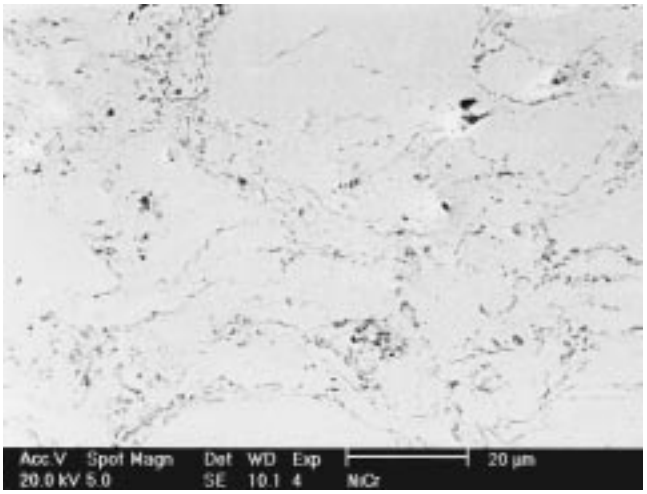

(a)

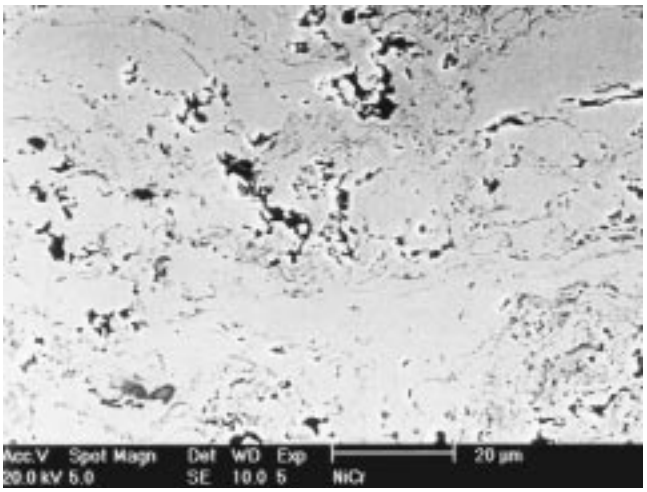

(b)

Fig. 7 SEM image of HVOF-sprayed Inconel 625 coating. **(a)** Before immersion test. **(b)** After one week immersion in 3.5 wt.% NaCl

to the 3.5 wt.% NaCl solution, indicating active corrosion behavior. At the same time, it was noted that a couple of hours after the beginning of the test, the first corrosion products appeared more or less evenly on the entire surface of the exposed coating. Perhaps because of interconnected pores, splat boundaries, and microcracks characteristic of sprayed coatings, the electrolyte quickly reached the substrate and corroded it, as shown in Fig. 6. If the sprayed coating structures are compared before and after the immersion test, as in the SEM images in Fig. 7, it can be seen that the coating material itself has corroded selectively. It seems that the deterioration of the coating has begun along splat boundaries and corroded the material nearby. Dent *et al.*[10] have noticed the same kind of degradation at splat boundaries in HVOF-sprayed Ni-Cr-Mo-B coating exposed to 0.5 M H_2SO_4, especially when significant oxidation had occurred during spraying. Edris *et al.*[11] have found out that HVOF-sprayed Inconel 625 coating includes a certain amount of low-alloy Ni-based metallic regions, which suffer from chromium depletion and the existence of which depend on the amount of oxidation (predominantly Cr_2O_3, but $NiCr_2O_4$ is also possible[10,11]). From Fig. 7, one can conclude that those low-alloy Ni-based regions are located right next to oxide layers (Cr_2O_3, $NiCr_2O_4$) between splats. However, the potential difference between Inconel 625 HVOF-coated and uncoated Fe 37 substrate was measured to be approximately 200 mV more negative for the uncoated Fe 37 substrate (Fig. 8). This indicates the more noble character of the sprayed coating than the substrate. When electrolyte connection is established between the coating and the substrate, a galvanic pair is generated, with the substrate acting as anode and the coating as cathode. In this case, the coating is cathodically protected and the substrate corrodes quickly (Fig. 6) due to electrolyte connection and unfavorable surface area ratio.

Laser-remelted coatings showed another type of behavior. In the case of 2250 W/600 mm/min coatings and 2250 W/500 mm/min coatings, the open circuit potential started to change to a more positive direction after exposure to electrolyte, indicating passive corrosion behavior. After one week of immersion, the surface of the exposed area was still free of any corrosion products. Open circuit potential was noted to be 700 mV more positive than that of uncoated Fe 37 substrate (Fig. 8.). Coatings

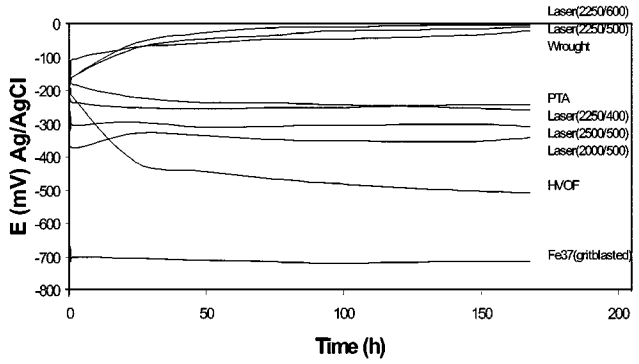

Fig. 8 Open circuit potential vs time for the wrought, PTA, laser-remelted, and HVOF-sprayed Inconel 625 alloy

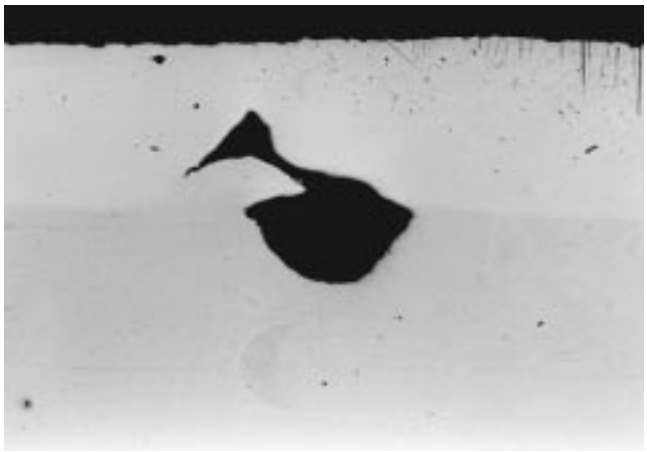

Fig. 9 Optical micrograph of remelted (2500 W, 500 mm/min) Inconel 625 coating after one week immersion in 3.5 wt.% NaCl. Coating thickness is 500 μm

remelted with parameters 2000/500, 2500/500, and 2250/400 allowed the electrolyte to pass the coating through a single interconnected pore, causing crevice corrosion-like behavior (Fig. 9). Corrosion products appeared from the substrate through this single pore to the surface a couple of hours after the beginning of the test. At the same time, it was noted that open circuit potential values decreased as in the case of the sprayed coating, being, however, 200 mV more positive than values of the sprayed coating/substrate system.

The reason for the defects such as cracks or porosity allowing the electrolyte to pass the remelted coating can be related to the properties of the substrate and/or laser processing parameters. Interconnecting pores are formed when atmospheric gases are dissolved in the melt pool during remelting and entrapped within the coating while rapid cooling takes place. At very high processing speeds, air bubbles do not have enough time to escape before solidification. On the other hand, at very low processing speeds, the amount of dissolved gases increases causing porosity.[6] In addition, low processing speeds lead to excessive melting and evaporation of possible inclusions/impurities in the substrate material, which is most probably the case at least in 2500/500 and 2250/400 remelted samples. In Fig. 9, the deteriorated area in the middle of coating hints also to compositional inhomogeneity due to Fe dilution from the substrate.

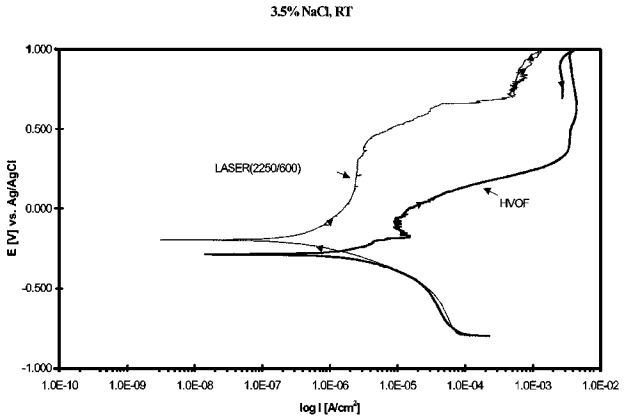

Fig. 10 Cyclic polarization curves of remelted (2250 W, 600 mm/min) and HVOF-sprayed Inconel 625 coatings

As a reference, immersion test and OCP measurements were also done with wrought and PTA samples. Wrought Inconel 625 exhibited passivation behavior identical to the best laser-remelted samples (2250/600 and 2250/500) and PTA showed active corrosion behavior, allowing the electrolyte to pass the coating and corrode the substrate in spite of markedly higher coating thickness (2.3 mm) in the PTA sample.

3.2 Electrochemical Measurements

Figure 10 shows the cyclic polarization curves for the laser-remelted sample with parameters 2250/600 and HVOF-sprayed coatings measured in 3.5 wt.% NaCl solution. The sprayed coating exhibits poorer corrosion resistance in the solution having lower corrosion potential (–288 mV versus Ag/AgCl) and higher corrosion current density (1.2×10^{-6} A/cm^2) compared to remelted (–197 mV versus Ag/AgCl, 3.6×10^{-7} A/cm^2) coating. Corrosion current densities were estimated from cyclic polarization curves. In addition, the HVOF-sprayed sample shows a rapid increase in current after narrow passivation area (from –200 to –60 mV versus Ag/AgCl), already at about –60 mV versus Ag/AgCl, which is breakdown potential. The remelted sample exhibits a rapid increase in current at +430 mV versus Ag/AgCl, indicating higher breakdown potential. The remelted sample also shows a substantially wider passivation region compared to the as-sprayed sample. A rapid increase in current usually means the breakdown of passivity in the passivation layer on the coating, indicating localized corrosion, commonly known as pitting or crevice corrosion. In this case of the remelted and sprayed samples, the rapid increase in current is probably not due to pitting, but uniform corrosion of the coating material itself in the transpassive region. In addition, both the curves showed negative hysteresis, which also does not support pitting corrosion. Moreover, the surfaces of the samples were examined visually after the cyclic polarization and both the exposed surfaces proved to be free of corrosion pits.

For comparison, the polarization curves of wrought Inconel 625 and PTA coating are displayed together with the remelted coating in Fig. 11 and 12. The corrosion performance of the remelted sample is very close to the corresponding wrought material. Corrosion potential and corrosion current density in the passive region are even slightly better in the case of the remelted

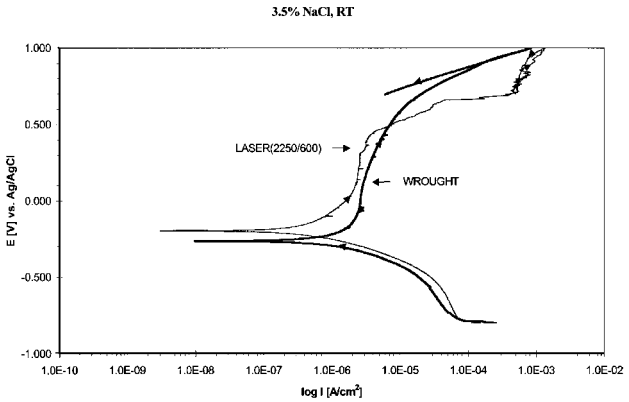

Fig. 11 Cyclic polarization curves of remelted (2250 W, 600 mm/min) Inconel 625 coating and wrought Inconel 625 alloy

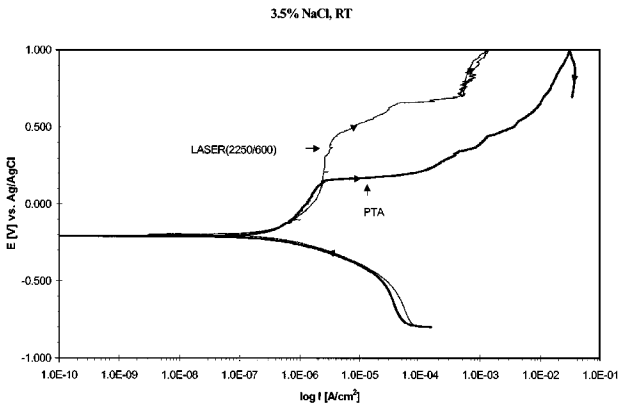

Fig. 12 Cyclic polarization curves of remelted (2250 W, 600 mm/min) and PTA Inconel 625 coatings

sample. The breakdown potential of the remelted sample is obvious at about +430 mV versus Ag/AgCl and lower than that of the wrought sample, for which it is difficult to point out the exact breakdown potential. Perhaps, it is more correct to say that the passivity of the wrought sample is maintained until about +600 mV versus Ag/AgCl. Compared to Inconel 625 PTA coating, the corrosion potentials and corrosion current densities are very similar. However, the remelted coating exhibits higher breakdown potential and a larger passivation region than the PTA coating. In addition, positive hysteresis of the PTA coating indicates pitting corrosion, which was also confirmed visually from the surface of the sample and under the gasket after cyclic polarization measurements.

The corrosion resistance of the coating/substrate system is more or less dominated by the substrate material if interconnected porosity, micropores, or microcracks exist in the coating material. From the above immersion test, open circuit potential, and cyclic polarization measurements, it can be said that the corrosion properties of the remelted (2250/600) sample were very close to corresponding wrought material. In the immersion test and open circuit potential measurements, remelted and wrought samples behaved identically, indicating the fact that the influence of substrate was neglected in the case of the remelted sample due to a uniform, pore- and crack-free coating layer. The

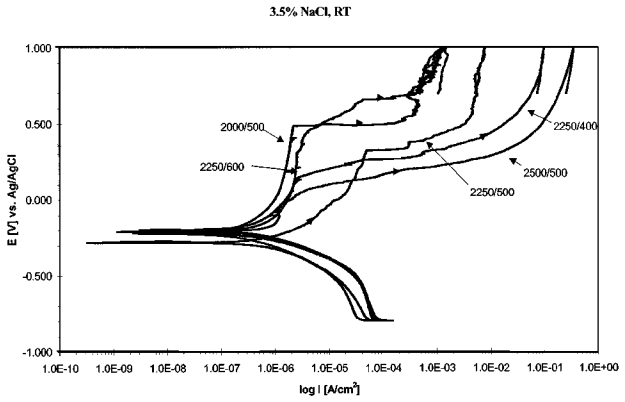

Fig. 13 Cyclic polarization curves of remelted Inconel 625 coatings with different parameters

minor difference in the breakdown of passivity on the surface of the remelted and PTA samples is perhaps related to the different microstructures or dissolution between coating and substrate. The influence of dissolution is particularly interesting and will be examined in the future, because it was noted that the breakdown potential decreased when the amount of specific surface energy was increased in remelting the samples.

The samples that received too much energy also showed visible pitting corrosion behavior on the surface of the coatings, crevice formation under the gasket, and positive hysteresis in cyclic polarization curves after the test (Fig. 13). Nakao and Nishimoto[12] have reported that the solidification rate of the laser-treated Inconel 625 alloy has great influence on pitting corrosion resistance. They varied the traverse speed of the laser beam to achieve different cooling rates. It was noted that pitting corrosion resistance of Inconel 625 was improved when solidification rates increased. At low traverse speed, that is, low solidification rate, the element distributions across the solidification cell appeared to be inhomogeneous. The cell cores suffered from the depletion of chromium and molybdenum, which are important elements for pitting corrosion resistance. At high solidification rates, the segregation of chromium and molybdenum has no time to take place. Cooper *et al.*[13] have also noted the detrimental effect of segregation of chromium and molybdenum on the corrosion performance of laser-treated Inconel 625 alloy in seawater. Depletion of chromium and molybdenum together with substrate dissolution can explain the results obtained from cyclic polarization measurements. The samples that absorbed the highest specific energy (2500/500, 2250/400, and PTA) and had the lowest solidification rate suffered from pitting corrosion. The results of the corrosion tests are summarized in Table 4. These results show clearly the decreasing tendency of breakdown potential with respect to the amount of energy absorbed by the substrate/coating system (laser 2250/600 and 2000/500 versus laser 2500/500, 2250/400, and PTA).

3.3 HT Oxidation Test

Microstructures of the tested samples revealed that HVOF-sprayed coating suffered from oxidation, whereas laser-remelted (2000/500) and PTA coatings did not show any deterioration of

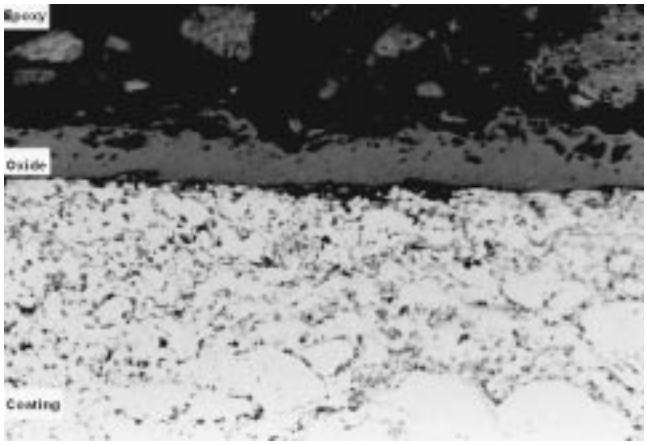

Fig. 14 Optical micrograph of HVOF-sprayed Inconel 625 coating after high-temperature oxidation test. Oxide layer thickness is 15 μm

Table 4 The results of corrosion test for Inconel 625 alloy

Sample	E_{corr} (mV)	I_{corr} (A/cm^2)	E_{bp} (mV)	E_{ocp} (mV)
Wrought	–264	$4.6 \cdot 10^{-7}$	+600	–22
HVOF	–288	$1.2 \cdot 10^{-6}$	–60	–526
PTA	–207	$3.1 \cdot 10^{-7}$	+154	–242
Laser (2250/600)	–197	$3.6 \cdot 10^{-7}$	+433	–3
Laser (2000/500)	–221	$1.8 \cdot 10^{-7}$	+487	–342
Laser (2250/500)	–282	$4.2 \cdot 10^{-7}$	+324	–8
Laser (2500/500)	–219	$3.0 \cdot 10^{-7}$	–30	–307
Laser (2250/400)	–209	$4.4 \cdot 10^{-7}$	+144	–259

the structure, acting in a way similar to the corresponding wrought material. It can be detected from Fig. 14 that the amount of oxidation along splat boundaries has increased during the test. The oxide layer, which seems to be relatively porous, formed on the surface of the sprayed coating has allowed the oxygen to diffuse through it and propagate along splat boundaries. The oxide layer formed on the surface of the coating has the thickness of about 15 μm. Remarkably thinner oxide layers were detected from the surface of laser-remelted (2000/500) and PTA coatings. The structure of the oxide layer with a thickness of 1 to 2 μm was difficult to analyze by optical microscopy, but it is obvious from the unchanged microstructures of the coatings that the oxide layer is very dense, giving excellent protection against oxidation at 800 °C in air atmosphere. Yang *et al.*[14] have reported similar results when flame-sprayed and laser-cladded NiCrSiB alloys were tested at 900 °C in atmosphere.

4. Conclusions

The tests performed in this study showed and confirmed the fact that the resistance of the sprayed coating to corrosion and high-temperature oxidation is still inferior compared to corresponding bulk material despite the use of one of the most advanced HVOF processes. The inhomogeneous structure, including oxide layers along splat boundaries and porosity, inherent to sprayed coating is responsible for limited corrosion and high-temperature oxidation performance, allowing electrolyte and oxygen to destroy the less noble substrate. In addition, the coating itself suffered from selective corrosion mainly along splat boundaries.

The laser remelting of the sprayed coating improved corrosion and high-temperature oxidation performance markedly, if appropriate processing parameters were chosen. Laser parameters (power and traverse speed in this case) generating too high a specific energy should be avoided, because of decreasing dilution (Fe) from substrate to coating, particularly the pitting corrosion resistance of the coating. The origin of pores, found in some of the remelted samples, needs to be examined in the future, especially the effect of possible inclusions near the substrate/coating interface. Nevertheless, it seems that it is possible to achieve an excellent performance equivalent to wrought Inconel 625 superalloy with laser remelting of sprayed coating by selection of appropriate laser remelting parameters.

Acknowledgments

The authors are grateful to The National Technology Agency TEKES, Valmet Corp., Ahlstrom Machinery Corp., and Imatra Steel Oy Ab for financial support of the present work.

References

1. D. Bacci and S. Tosto: *Proc. AGARD Conf. Advanced Fabrication Processes*, Florence, Italy, Sept. 1978, 1979, vol. CP-256, p. 10.
2. H. Bhat, H. Herman, and C.J. Coyle: in *Laser in Processing Materials*, TMS-AIME, Warrendale, PA, 1983, pp. 176-83.
3. T.A. Mahank, J. Singh, and A.K. Kulkarni: *Mater. Manufacturing Processes*, 1998, vol. 13 (6), pp. 829-39.
4. N. Eguchi, Z. Zhou, H. Shirasawa, and A. Ohmori: in *Thermal Spray: Meeting the Challenges of the 21st Century*, C. Coddet, ed., ASM International, Materials Park, OH, 1998, pp. 1517-22.
5. R. Streiff, M. Pons, and P. Mazars: *Surf. Coatings Technol.*, 1987, vol. 32, pp. 85-95.
6. G.L. Goswami, D. Kumar, A.K. Grover, A.L. Pappachan *et al.: Surf. Eng.*, 1999, vol. 15 (1), pp. 65-70.
7. G.Y. Liang and T.T. Wong: *Surf. Coatings Technol.*, 1997, vol. 89, pp. 121-26.
8. Z. Dawei, T. Li, and T. C. Lei: *Surf. Coatings Technol.*, 1998, vol. 110, pp. 81-85.
9. J.K. Shin, J.H. Suh, J.S. Kim, and S.-J.L. Kang: *Surf. Coatings Technol.*, 1998, vol. 107, pp. 94-100.
10. A.H. Dent, A.J. Horlock, D.G. McCartney, and S.J. Harris: *J. Thermal Spray Technol.*, 1999, vol. 8 (3), pp. 399-404.
11. H. Edris, D.G. McCartney, and A.J. Sturgeon: *J. Mater. Sci.*, 1997, vol. 32, pp. 863-72.
12. Y. Nakao and K. Nishimoto: *Iron Steel Inst. Jpn. Int.*, 1993, vol. 33, pp. 934-40.
13. K.P. Cooper, P. Slebodnick, and E.D. Thomas: *Mater. Sci. Eng.*, 1996, vol. A206, pp. 138-49.
14. X.C. Yang, Y.H. Yan, X.K. Wang and H.W. Gu: in *Applications of Lasers and Electro-optics*, ICALEO 87, San Diego, CA, 1987, pp. 209-20.